# Attosecond nanoplasmonic-field microscope

MARK I. STOCKMAN[1,2]*, MATTHIAS F. KLING[2], ULF KLEINEBERG[3] AND FERENC KRAUSZ[2,3]*

[1]Department of Physics and Astronomy, Georgia State University, Atlanta, Georgia 30303, USA
[2]Max-Planck-Institut für Quantenoptik, Hans-Kopfermann-Straße 1, D-85748 Garching, Germany
[3]Ludwig-Maximilians-Universität München, Department für Physik, Am Coulombwall 1, D-85748 Garching, Germany
*e-mail: mstockman@gsu.edu; ferenc.krausz@mpq.mpg.de

**Nanoplasmonics deals with collective electronic dynamics on the surface of metal nanostructures, which arises as a result of excitations called surface plasmons. This field, which has recently undergone rapid growth, could benefit applications such as computing and information storage on the nanoscale, the ultrasensitive detection and spectroscopy of physical, chemical and biological nanosized objects, and the development of optoelectronic devices. Because of their broad spectral bandwidth, surface plasmons undergo ultrafast dynamics with timescales as short as a few hundred attoseconds. So far, the spatiotemporal dynamics of optical fields localized on the nanoscale has been hidden from direct access in the real space and time domain. Here, we propose an approach that will, for the first time, provide direct, non-invasive access to the nanoplasmonic collective dynamics, with nanometre-scale spatial resolution and temporal resolution on the order of 100 attoseconds. The method, which combines photoelectron emission microscopy and attosecond streaking spectroscopy, offers a valuable way of probing nanolocalized optical fields that will be interesting both from a fundamental point of view and in light of the existing and potential applications of nanoplasmonics.**

Recently, significant attention has been devoted to the development of attosecond science and technology, in particular regarding pulse generation, physical-system excitation, detection, spectroscopy and electron-motion control on the attosecond timescale[1–13]. In nanoscience, which is another rapidly evolving field, an important issue is the study and exploitation of effects that are both ultrafast and localized on the nanoscale. The localization length of surface plasmon eigenmodes in nanoplasmonic systems is determined by the size of the constituent nanoparticles and can be on the order of several nanometres[14]. Furthermore, the relaxation rate of the surface plasmon polarization is in the $10-100$ fs range across the plasmonic spectrum, allowing coherent control of nanoscale energy localization with femtosecond laser light[15–25]. Importantly, collective motion in nanoplasmonic systems unfolds on much shorter attosecond timescales, as defined by the inverse spectral bandwidth of the plasmonic resonant region. In this paper we propose an approach that enables direct measurement of the spatiotemporal dynamics of nanolocalized optical fields with 100-as temporal resolution and nanometre-scale spatial resolution. Nanoplasmonic fields could be used in place of electrons in ultrafast computation and information storage on the nanoscale, where the fields act as the medium that carries, processes and stores information.

The proposed attosecond nanoplasmonic-field microscope combines two modern techniques: photoelectron emission microscopy and attosecond streaking spectroscopy[26]. A plasmonic nanostructure is excited by an intense, waveform-controlled field in the optical spectral range that drives collective electron oscillations (the quantum of which is called a surface plasmon). This generates optical fields localized on the nanometre scale, which we will refer to as nanolocalized optical fields. An

attosecond extreme ultraviolet (XUV) pulse, which is produced from and synchronized with the driving optical pulse, is then sent to the system. This XUV pulse produces photoelectrons that, owing to their large energy and short emission time (determined by the attosecond-pulse duration), escape from the nanometre-sized regions of local electric fields enhanced by plasmon resonances within a fraction of the oscillation period of the driven plasmonic field. The ultrashort escape time implies a final energy change of the emitted photoelectrons that is proportional to the local electric potential at the surface at the instant of electron release. This is in sharp contrast to previous attosecond streaking experiments performed in macroscopic volumes of gas-phase media, where the electron escape times are longer than the optical period; consequently, the change in electron energy probes the vector potential of the optical field[26]. For nanoplasmonic systems, the imaging of the emitted XUV-induced photoelectrons by an energy-resolving photoelectron emission microscope (PEEM) probes the electric-field potential at the surface as a function of the XUV-pulse incidence time and the position at the surface with an attosecond temporal and nanometre-scale spatial resolution.

Schematically our approach is illustrated in Fig. 1. Similarly to ref. 27, it is based on the use of attosecond XUV pulses that are synchronized with the waveform-controlled optical fields[5], which are used here to drive the nanolocalized excitations of a plasmonic nanostructure. A metal (plasmonic) nanosystem is driven by an optical ultrashort laser pulse with frequency within the range of the plasmonic resonances (from near UV to near infrared, NIR). The wavelength of the optical radiation is orders of magnitude greater than the characteristic size of the nanosystem, which we assume to be on the order of tens of
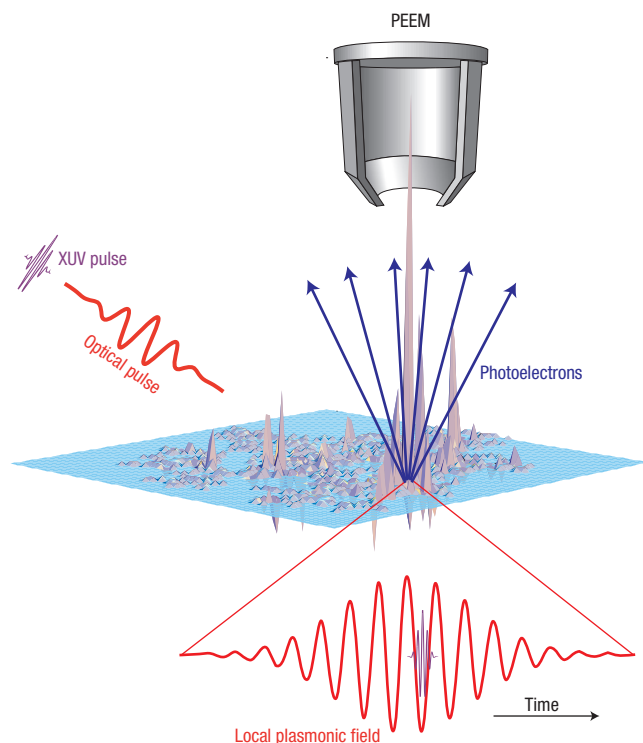
**Figure 1 Schematic of the system and photoprocesses.** The nanosystem is shown in a plane denoted in light blue. Instantaneous local fields, which are excited by the optical pulse, are shown as a three-dimensional plot. The local optical field at a point of the maximum field ('hottest spot') is shown as a function of time by a red waveform, enhanced with respect to the excitation field. The application of an XUV pulse is shown by a violet waveform that is temporally delayed with respect to the excitation field. The XUV excitation causes the emission of photoelectrons shown by the blue arrows, which are accelerated by the local plasmonic potential. They are detected with spatial and energy resolution by a PEEM.

nanometres. The plasmonic nanosystem responds to the almost uniform field of the optical excitation with 'hot spots', where the local fields are enhanced with respect to the excitation field by a factor that depends on the quality of the localized surface plasmon resonances and can be as high as a few hundred for silver nanosystems. These hot spots are indicated as the peaks of the local field amplitude in Fig. 1. For the highest of these peaks ('hottest spot'), we show (as the red waveform) the temporal dynamics of the local electric field. Similar to direct measurements of the optical field's instantaneous magnitude[27], an attosecond XUV pulse is incident on the system synchronously with the optical excitation waveform. It causes the photoemission of electrons whose energy is high enough to select them from the background of above-threshold ionization (ATI) and multiphoton emission created by the optical field.

These XUV electrons are accelerated by the local plasmonic electric fields, which define their energies. Imaging such a system in a PEEM with energy resolution will allow one to see the hot spots and find the instantaneous magnitude of the plasmonic field at the site and time of the emission. As the emission instant is defined by the XUV pulse, this would allow one to measure the complete spatiotemporal dynamics of the local fields. The corresponding spatial resolution is defined solely by the electron optics of the PEEM (the de Broglie wavelength of the XUV

electrons is much smaller and is not a limiting factor) and can realistically be on the order of nanometres. The temporal resolution is determined by the duration of the attosecond pulse and the time of flight of the photoelectrons through the local-field region, which can be on the order of (a few) hundred attoseconds. Very importantly, this proposed approach to the visualization of the attosecond–nanometre dynamics is non-invasive with respect to the plasmonic fields because of the low power of the XUV pulses.

## ELECTRON ACCELERATION BY NANOPLASMONIC FIELDS

Different regimes of the electron emission by an XUV pulse will now be discussed to identify those realistic for our conditions and conducive to our goals. The escape velocity for an electron can be estimated as $v_e = \sqrt{2(\hbar\omega_{XUV} - W_f)/m}$, where $m$ is the electron mass, $\omega_{XUV}$ is the frequency of the XUV pulse, $W_f$ is the metal workfunction and $\hbar$ is the reduced Planck's constant. The electron escape time from a region of local field of size $b$ is $\tau_e = b/v_e$. The most important case for our purposes is the one to be called a regime of instantaneous acceleration, when an electron leaves the local-field region much faster than this field oscillates in time, that is,

$$\tau_e \ll T \qquad (1)$$

where $T = 2\pi/\omega$ is a characteristic period of the optical excitation, and $\omega$ is the excitation-pulse carrier frequency.

Under this condition, an electron is driven by a nearly frozen, instantaneous local electrostatic potential $\phi(\mathbf{r}, t_{XUV})$, where $t_{XUV}$ is the emission time defined with a sufficient precision by the incidence time of the XUV pulse. The final kinetic energy of an electron, which is measured by the PEEM, is found from energy conservation,

$$E_{XUV}(\mathbf{r}, t_{XUV}) = \hbar\omega_{XUV} - W_f + e\phi(\mathbf{r}, t_{XUV}) \qquad (2)$$

where $e$ is the electron charge and $\mathbf{r}$ the emission point. In sharp contrast to attosecond streaking in the gas phase[26], this energy does not depend on the initial momentum of the photoelectron or its subsequent flight trajectory.

Estimates for the currently available XUV pulse parameters are chosen as follows[28]: pulse duration $\tau_p = 170$ as and photon energy $\hbar\omega_{XUV} = 91$ eV. In such a case, assuming the workfunction $W_f = 5$ eV, we obtain the escape velocity $v_e = 5 \times 10^8$ cm s$^{-1}$ and the escape time for the localization distance $b = 1$ nm as $\tau_e = 180$ as. Considering an NIR driving pulse with a characteristic period $T \sim 3$ fs, we see that the instantaneous-regime condition (1) is well satisfied for an optical field localization length up to several nanometres. Temporal resolution $\tau_r$ of the attosecond plasmonic-field microscope is determined by both flight time $\tau_e$ through the region of nanolocalized optical fields and the duration $\tau_p$ of the XUV pulse itself, $\tau_r \sim \tau_e + \tau_p$. For an NIR driving field and $b \lesssim 3$ nm, this resolution is sufficient, $\tau_r \ll T$. For visible excitation and plasmonic frequencies, sufficient temporal resolution can be achieved in the future with attosecond pulses delivered with photon energy $\hbar\omega_{XUV}$ of several hundred eV to a keV and duration below 100 as.

In the instantaneous regime (1) and (2), we can collect a large number of electrons leaving the surface without sacrificing the temporal resolution provided by the attosecond streaking, owing to the fact that the electron energy shift is independent of the emission angle. This is in sharp contrast to the regime of the multiple electron oscillations induced by the optical field

(which, for brevity, will be referred to as the 'oscillatory regime'). The oscillatory regime was dominant in the earlier experiments with the gas phase[27,29]. In this regime, the dwelling (escape) time of an emitted electron in the region of the streaking optical field is large enough, $\tau_e \gtrsim T$. In that case, the motion is governed not by the scalar potential but by the vector potential $\mathbf{A}(t)$, and the electron velocity $\mathbf{v}$ undergoes many oscillations[26]. As a result, the field-dependent part of the final electron energy $E_{XUV}$ is dominated by a term $\Delta E_{XUV} = (e/mc)\mathbf{v}_0\mathbf{A}(t_{XUV})$ that depends on the direction of emission velocity $\mathbf{v}_0$. In energy-resolved microscopy, this would lead to a drastic decrease in the intensity of the spectral features and their smearing-out.

The oscillatory regime of the electron acceleration also took place in the experiments[30,31] where electrons were emitted from a plasmonic metal surface in a multiphoton process excited by an NIR field. After the emission, these electrons are accelerated by local fields of the surface plasmon polaritons (SPPs). The major difference between these experiments and our proposed attosecond microscope arises from the fact that the electron emission energy of refs 30 and 31 is much lower, and the field localization radius characteristic of SPPs is much larger than in the present case, $b \sim 1\,\mu m$. Thus, in those experiments, the Fermi edge of the emitted electron distribution was significantly smeared out.

In contrast, in our proposed approach, $E_{XUV}$ of equation (2) does not depend on the direction of emission or a specific trajectory of the electron motion. This will allow electrons to be collected in a wide solid angle of emission, which is of utmost importance in providing a good signal-to-noise ratio, without sacrificing the energy resolution (and, consequently, the accuracy of the plasmonic potential measurement). It will be shown in the following that for the moderate optical intensities assumed, the shift of the electron energy due to the acceleration in the local field $\Delta E_{XUV} = e\phi$ is on the order of 10 eV and should be easily measurable. Thus, this instantaneous regime is ideal for the direct measurement of the attosecond–nanometre dynamics of the local plasmonic potential and is the most desirable. However, at present it can only be achieved for strongly localized plasmonic fields whose extension should not exceed a few nanometres. This restriction applies only until attosecond pulses become available at much higher photon energies ($\sim 1$ keV and beyond).

## CALCULATIONS AND RESULTS

### PLANAR METAL NANOSTRUCTURES IN THE ATTOSECOND PLASMONIC-FIELD MICROSCOPE

Concentrating on this most important case of the instantaneous acceleration described by equations (1) and (2), we start with a model of a silver[32] random planar composite (whose geometry will be described in the next paragraph). We apply an $s$-polarized (along the $z$-direction), waveform-controlled[5], 5.5-fs optical pulse as shown in Fig. 2a. We have computed the electric potential $\phi(\mathbf{r}, t)$ using the quasi-static spectral-expansion Green's function method[14,15,33]. The excitation intensity is kept at a moderate level of $I = 10$ GW cm$^{-2}$ to ensure non-damaging conditions of the excitation. The carrier frequency of the optical (NIR) pulse is chosen to be 1.55 eV (corresponding to an 800-nm vacuum wavelength). The temporal kinetics of the local field at a site where it reaches its global maximum is displayed in Fig. 2b. It shows the initial period of the driven oscillations for $t < 20$ fs, where the response closely reproduces, albeit with a delay, the 5-fs excitation pulse, which reflects the bandwidth of this plasmonic system. At longer times, after the end of the excitation pulse, the free-induction evolution shows the interference
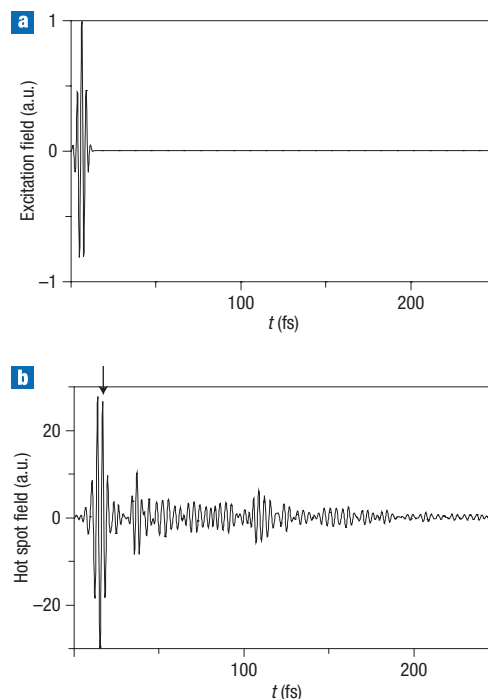
**Figure 2 Excitation field and kinetics of the local field at a hot spot.** **a**, Excitation field as a function of time. **b**, Local field at the position of the maximum ('hottest spot') in Fig. 3b as a function of time. The field magnitude is shown relative to the amplitude of the excitation pulse, which is set to 1. The vertical arrow denotes the oscillation period within which an XUV pulse is applied to probe the local field.

beatings of several plasmonic eigenmodes. The maximum enhancement in this hot spot is $Q \approx 30$.

The random planar composite is generated as a collection of uncorrelated silver cubes (monomers) positioned on a plane in vacuum, which is illustrated in Fig. 3a for a monomer size of 4 nm. As is characteristic of plasmonic nanosystems, there are hot spots of local fields induced by the optical excitation. The local field dynamics is shown in Fig. 2b for the 'hottest spot', where the local field reaches its global maximum in space and time. We assume that an XUV attosecond pulse is incident at this system delayed with respect to the waveform-controlled[5] driving field in such a way that it probes the system close to the instance of the local field maximum (indicated by an arrow in Fig. 2b). According to equation (2), we compute the energy shift of an electron emitted by such an XUV pulse, which is due to the acceleration in the local plasmonic fields, as $\Delta E_{XUV}(\mathbf{r}, t_{XUV}) = e\phi(\mathbf{r}, t_{XUV})$. We assume that these photoelectrons are spatially resolved by a PEEM and show in Fig. 3b–f a series of the electron energy distributions with an interval of $\Delta t_{XUV} \approx 200-400$ as during a half period of the driving field. The distributions are shown as a three-dimensional map in panel 3b and as topographic maps in panels c–f. Even for the moderate excitation intensities used, the energy shift $|\Delta E_{XUV}|$ in hot spots of the plasmonic potential is rather large ($\sim 10$ eV) and, consequently, relatively easily measurable. There is a pronounced nanometre–attosecond kinetics of the electron energy observed in these distributions, with sharp hot spots indicative of those of the local fields. These hot spots are concentrated around the edges and voids of the metal nanostructure as is a general trend in nanoplasmonics. (See Supplementary Information for more details,
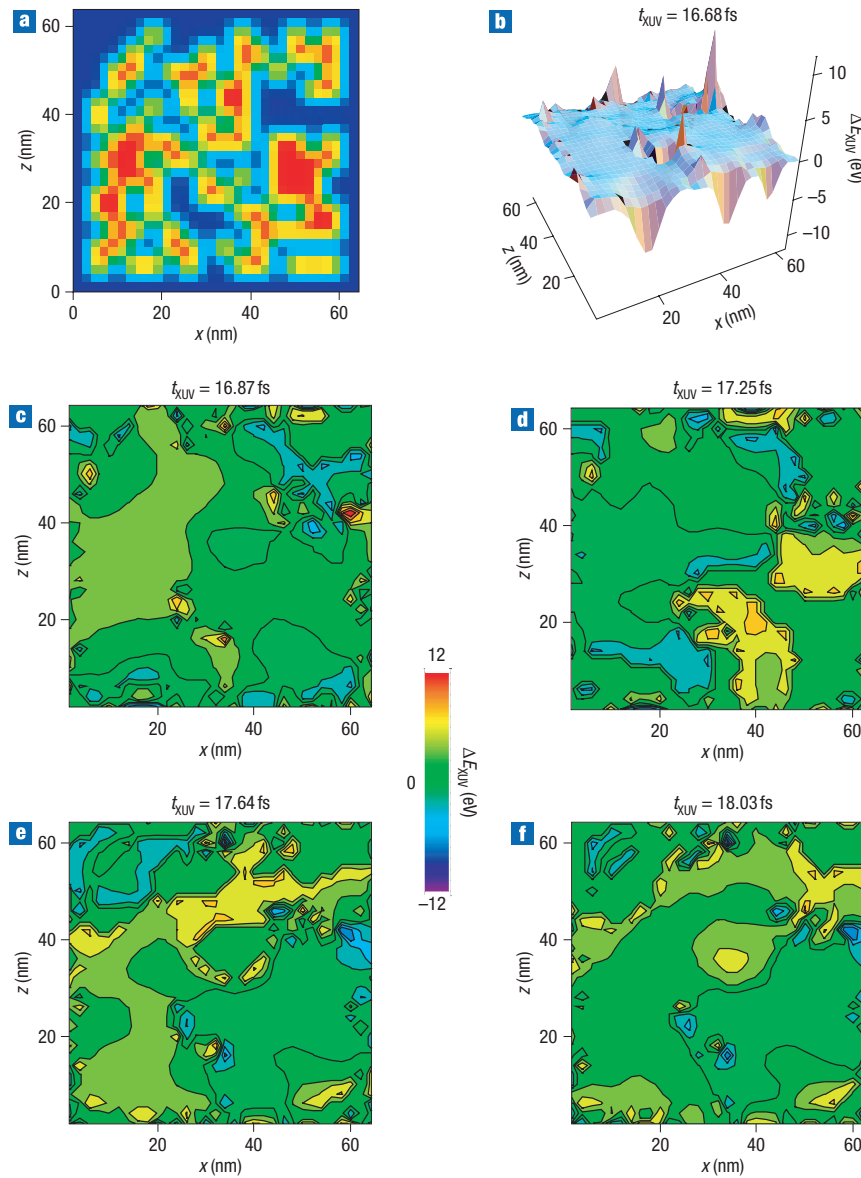
**Figure 3 Topography of a nanosystem and spatiotemporal kinetics of the local field potential as detected by the attosecond plasmonic-field microscope.**
Intensity of the excitation optical pulse $I = 10$ GW cm$^{-2}$, and photon energy $\hbar\omega = 1.55$ eV. **a**, Topography of the nanosystem: random planar composite consisting of 4 nm $\times$ 4 nm $\times$ 4 nm silver cubes arranged on a plane with fill factor 0.5. This composite is smoothed to within 2 nm to improve numerical precision. **b–f**, Distributions of the energy shift $\Delta E_{XUV}$ of electrons emitted by the XUV pulse in the plane of this nanostructure shown for different moments $t_{XUV}$ (as indicated in the panels) of the XUV pulse incidence within the half cycle of local field oscillations. **b**, A three-dimensional map. **c–f**, Topographic colour maps showing details of the nanometre–attosecond spatiotemporal kinetics.

in the movie Attosecond_Electron_Energy_tm5.5_130_180_.2mov of the XUV electron energy distribution for a longer, 30-fs interval of the evolution.)

Note that after leaving the region of the enhanced local fields, the electron's motion is oscillatory and defined by the vector potential of the excitation field in the empty space. The maximum change of the electron energy due to this motion is given by a leading term $(\hbar\omega_{XUV} - W_f)\xi$, where $\xi \leq \sqrt{\{8\pi e^2 I(t_{XUV})/[mc\omega^2(\hbar\omega_{XUV} - W_f)]\}}$ is a dimensionless parameter ($c$ is the speed of light in a vacuum); it is assumed that $\xi \ll 1$. In fact, for $I = 10$ GW cm$^{-2}$, $\xi \leq 5 \times 10^{-3}$; thus, this energy change in the free space is small enough and can be safely neglected.

## XUV ELECTRON ENERGIES FOR NANOSHELLS

It may also be useful to carry out the first experiments without spatial resolution by studying the energy distribution of the XUV-emitted electrons. As an example, we consider in such a case a much simpler nanoplasmonic system such as metal nanoshells[34]. Such nanoshells are frequency tunable by adjusting their aspect ratio $A$ (the ratio of the inner to outer shell radius). Assuming small shell radius ($R \lesssim 10$ nm), we can use the quasi-electrostatic approximation where the corresponding solutions are obtained in a simple analytical form.

Consider for instance a silver nanoshell of $R = 2.5$ nm on a core with a permittivity of $\varepsilon = 10$, which is resonant to 800 nm radiation for $A = 0.831$. For such a case, the energy shift of the
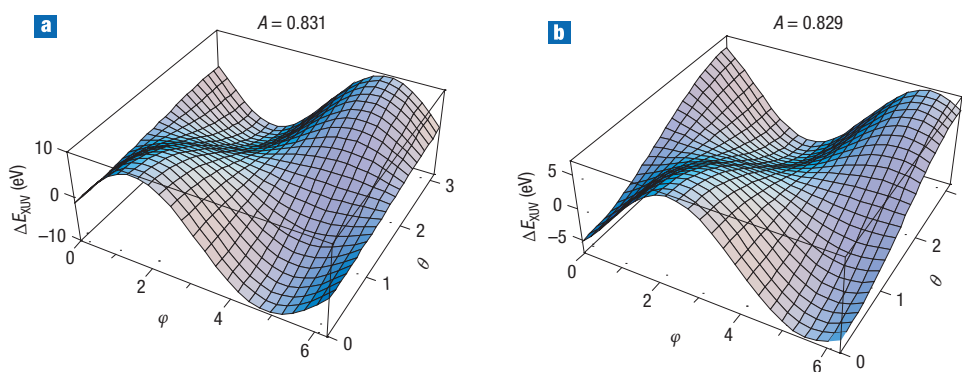
**Figure 4** Energy shift of electrons emitted from the surface of silver nanoshells as a function of the azimuthal angle $\theta$ of the emission point and the phase $\varphi$ of the delay between the driving optical radiation and the probing attosecond XUV pulse. The intensity of the excitation optical pulse is $I = 10 \, \text{GW cm}^{-2}$, the photon energy is $\hbar\omega = 1.55 \, \text{eV}$ and the outer radius of the nanoshells is $R = 2.5 \, \text{nm}$. **a,b**, Data for the nanoshells with aspect ratio $A = 0.831$ (**a**) and for $A = 0.829$ (**b**).

electrons is shown in Fig. 4, as a function of both the phase delay $\varphi$ between the driving NIR field and the incident attosecond pulse, and the azimuthal angle $\theta$ of the electron-emission point (for $I = 10 \, \text{GW cm}^{-2}$ and $\hbar\omega = 1.55 \, \text{eV}$). To avoid any confusion, we emphasize that the electron energy does not depend on the direction of the electron velocity but only on the azimuth of a point at the nanoshell surface from which the emission took place.

In the exact resonance for Fig. 4a, the maximum shift is $|\Delta E_{\text{XUV}}| \approx 10 \, \text{eV}$, on the same order as for the random planar composite above. The maximum is reached for $\varphi = \pi/2$, as expected for resonant excitation. The nanoshell resonance is very sharp; therefore, a small change of $A$ to a value of 0.829 detunes the resonance and leads to a significant reduction in the magnitude of the effect and a shift in its phase dependence (compare with Fig. 4b).

### DISCUSSION AND CONCLUSIONS

The state-of-the-art of attosecond technology for the attosecond plasmonic-field microscope proposed in this paper is represented by $\tau_\text{p} = 170 \, \text{as}$, $\hbar\omega_{\text{XUV}} = 93 \, \text{eV}$ XUV pulses containing $\gtrsim \times 10^6$ photons and delivered at a 3-kHz repetition rate[28,35]. As has been demonstrated earlier, such XUV pulses can be focused to a spot diameter of 2 μm (ref. 36).

The signal-to-noise ratio of the proposed attosecond nanoplasmonic-field microscope is limited by the electron currents that can be obtained from nanoscopic surface areas for the presently available intensities of the XUV sources[28,35]. In Materials and Methods the XUV photoelectron current emitted per 1-nm² area of the nanosystem surface is estimated. The number of photoelectrons per unit area of the nanosystem surface and unit time of observation (photoelectron fluence) is $j \sim 15 \, \text{nm}^{-2} \, \text{s}^{-1}$ for gold and $j \sim 10 \, \text{nm}^{-2} \, \text{s}^{-1}$ for silver. For the spatial resolution of PEEM available at present, $r \sim 10 \, \text{nm}$, this yields the electron flux from the area of resolution as $N' = \pi r^2 j \approx 4{,}500 \, \text{s}^{-1}$ for gold and $N' \sim 3{,}000 \, \text{s}^{-1}$ for silver. Such electron counts should not pose any problem for detection with PEEM.

Future steps towards the experimental implementation of the attosecond nanoplasmonic field microscope will use ultrashort pulsed XUV radiation with photon energies exceeding $\hbar\omega_{\text{XUV}} = 100 \, \text{eV}$. At present, single-attosecond XUV pulses are obtained by high-harmonic generation driven by a few-cycle waveform-stabilized Ti:sapphire laser pulse (800 nm, 5 fs) in a Ne gas jet target. Selecting a broadband (~9 eV full-width at-half-maximum (FWHM), centre frequency 91 eV) spectrum from the harmonic plateau range close to its cut-off by means of a Mo/Si multilayer-coated XUV mirror, single-attosecond XUV pulses have been extracted and pulse duration down to 250 as FWHM has been experimentally verified[7]. Improvements (broader-band mirrors) have yielded pulses shorter than 200 as. This offers a temporal resolution of at least 100 as. The excitation optical pulse and the probing XUV pulse are refocused to the sample by means of an interferometric double-mirror configuration allowing for controlled, variable time delays with 10-as steps. The spatially and energy-resolved detection of photoelectrons is achieved using a PEEM that is equipped with a flight drift tube followed by a two-dimensional delay-line detector. The spatial resolution of this time-resolved PEEM is limited by the electron optics to 20 nm. Silver and gold samples have been grown (see Supplementary Information for details, Experimental_Steps.pdf).

To conclude, we have proposed and developed a theory for an attosecond nanoplasmonic-field microscope. The main advantage of such a microscope is that it is non-invasive with respect to the nanoplasmonic fields. The principle of this microscope is based on the photoemission of electrons by an XUV attosecond pulse that is synchronized with a waveform-stabilized driving optical field. Information about the nanoplasmonic fields is imprinted in the energy of the XUV-emitted electrons owing to their acceleration in the instantaneous electrostatic potential of the surface plasmon oscillations excited by the optical field.

Our proposed microscope will open up unique possibilities to directly study and control ultrafast photoprocesses in surface plasmonic nanosystems and circuits. It images the local nanoplasmonic field in real space with nanometre-scale spatial resolution and in real time with ~100 as temporal resolution. This approach will be especially important in ultrafast nanoplasmonic systems where very tight localization of optical fields occurs, for example, when a shaped pulse of radiation induces nanolocalized fields at a desired nanosite. The microscope could also be used to study various plasmon-enhanced photoprocesses such as femtosecond photochemistry, light detection, and solar energy conversion where the processes of the energy transfer can be ultrafast. For example, with nanoplasmonic antennas, which couple together molecular and semiconductor systems with external fields, the ultrafast kinetics

of the energy exchange can be studied through the corresponding kinetics of the nanoplasmonic fields.

One of the most important potential uses of the attosecond nanoplasmonic-field microscope will be in the design and study of elements and devices for ultrafast and ultradense (at the nanoscale) optical and optoelectronic information processing and storage. To bring practical advantages over existing electronic and optoelectronic technology, such nanoscale devices must necessarily be ultrafast (with a subpicosecond or femtosecond response time). Examples of such devices include optical nanotransistors, memory cells, nanoplasmonic media for the mass storage of information, and nanoplasmonic interconnects where both the nanolocalization of energy and its ultrafast temporal kinetics are important.

## MATERIALS AND METHODS

Here we estimate the XUV electron photocurrent that can be obtained per 1-nm$^2$ area of the nanosystem metal surface. We adopt the values of the XUV photon flux for state-of-the-art XUV pulses[28,35]: $J_{XUV} \sim 10^9$ s$^{-1}$ (the flux averaged over time). The XUV pulses can be focused[36] to a spot with a radius $R \sim 1$ μm. This yields an XUV photon fluence $I_X \sim 8 \times 10^{16}$ cm$^{-2}$ s$^{-1}$. For $\hbar\omega_{XUV} = 91$ eV photon energy, the photoionization cross-section per atom for silver is $\sigma_a = 7.1$ Mb (ref. 37) and for gold is $\sigma_a = 10.9$ Mb (refs 37, 38).

Consider emission from an area $a = 1$ nm$^2$. For electron energies $\sim 100$ eV, the elastic escape depth (from which electrons come without losing their energy to collisions) is $h = 0.5$ nm (ref 39). The total photoemission cross-section from atoms within this elastic depth and area $a$ is $\sigma_{tot} = \rho a h \sigma_a$, where $\rho$ is the number density of atoms. From this we obtain the expected values of XUV photoelectron fluence $j \sim 15$ nm$^{-2}$ s$^{-1}$ for gold and $j \sim 10$ nm$^{-2}$ s$^{-1}$ for silver.

## References

1. Paul, P. M. *et al.* Observation of a train of attosecond pulses from high harmonic generation. *Science* **292**, 1689−1692 (2001).
2. Hentschel, M. *et al.* Attosecond metrology. *Nature* **414**, 509−513 (2001).
3. Niikura, H. *et al.* Sub-laser-cycle electron pulses for probing molecular dynamics. *Nature* **417**, 917−922 (2002).
4. Drescher, M. *et al.* Time-resolved atomic inner-shell spectroscopy. *Nature* **419**, 803−807 (2002).
5. Baltuska, A. *et al.* Attosecond control of electronic processes by intense light fields. *Nature* **421**, 611−615 (2003).
6. Niikura, H. *et al.* Probing molecular dynamics with attosecond resolution using correlated wave packet pairs. *Nature* **421**, 826−829 (2003).
7. Kienberger, R. *et al.* Atomic transient recorder. *Nature* **427**, 817−821 (2004).
8. Sekikawa, T., Kosuge, A., Kanai, T. & Watanabe, S. Nonlinear optics in the extreme ultraviolet. *Nature* **432**, 605−608 (2004).
9. Lopez-Martens, R. *et al.* Amplitude and phase control of attosecond light pulses. *Phys. Rev. Lett.* **94**, 033001 (2005).
10. Baker, S. *et al.* Probing proton dynamics in molecules on an attosecond time scale. *Science* **312**, 424−427 (2006).
11. Dudovich, N. *et al.* Measuring and controlling the birth of attosecond XUV pulses. *Nature Phys.* **2**, 781−786 (2006).
12. Sansone, G. *et al.* Isolated single-cycle attosecond pulses. *Science* **314**, 443−446 (2006).
13. Kling, M. F. *et al.* Control of electron localization in molecular dissociation. *Science* **312**, 246−248 (2006).
14. Stockman, M. I., Faleev, S. V. & Bergman, D. J. Localization versus delocalization of surface plasmons in nanosystems: Can one state have both characteristics? *Phys. Rev. Lett.* **87**, 167401 (2001).
15. Stockman, M. I., Faleev, S. V. & Bergman, D. J. Coherent control of femtosecond energy localization in nanosystems. *Phys. Rev. Lett.* **88**, 067402 (2002).
16. Bergman, D. J. & Stockman, M. I. Surface plasmon amplification by stimulated emission of radiation: Quantum generation of coherent surface plasmons in nanosystems. *Phys. Rev. Lett.* **90**, 027402 (2003).
17. Lehmann, J. *et al.* Surface plasmon dynamics in silver nanoparticles studied by femtosecond time-resolved photoemission. *Phys. Rev. Lett.* **85**, 2921−2924 (2000).
18. Zentgraf, T., Christ, A., Kuhl, J. & Giessen, H. Tailoring the ultrafast dephasing of quasiparticles in metallic photonic crystals. *Phys. Rev. Lett.* **93**, 243901 (2004).
19. Kubo, A. *et al.* Femtosecond imaging of surface plasmon dynamics in a nanostructured silver film. *Nano Lett.* **5**, 1123−1127 (2005).
20. Stockman, M. I. & Hewageegana, P. Nanolocalized nonlinear electron photoemission under coherent control. *Nano Lett.* **5**, 2325−2329 (2005).
21. Brixner, T. *et al.* Quantum control by ultrafast polarization shaping. *Phys. Rev. Lett.* **92**, 208301 (2004).
22. Brixner, T., d. Abajo, F. J. G., Schneider, J. & Pfeiffer, W. Nanoscopic ultrafast space−time-resolved spectroscopy. *Phys. Rev. Lett.* **95**, 093901 (2005).
23. Sukharev, M. & Seideman, T. Phase and polarization control as a route to plasmonic nanodevices. *Nano Lett.* **6**, 715−719 (2006).
24. Aeschlimann, M. *et al.* Adaptive subwavelength control of nano-optical fields. *Nature* **446**, 301−304 (2007).
25. Pelton, M., Liu, M. Z., Park, S., Scherer, N. F. & Guyot-Sionnest, P. Ultrafast resonant optical scattering from single gold nanorods: Large nonlinearities and plasmon saturation. *Phys. Rev. B* **73**, 155419 (2006).
26. Corkum, P. B. & Krausz, F. Attosecond science. *Nature Phys.* **3**, 381−387 (2007).
27. Goulielmakis, E. *et al.* Direct measurement of light waves. *Science* **305**, 1267−1269 (2004).
28. Schultze, M. *et al.* Powerful 170-attosecond XUV pulses generated with few-cycle laser pulses and broadband multilayer optics. *New J. Phys.* **9**, 243 (2007).
29. Drescher, M. *et al.* X-ray pulses approaching the attosecond frontier. *Science* **291**, 1923−1927 (2001).
30. Kupersztych, J., Monchicourt, P. & Raynaud, M. Ponderomotive acceleration of photoelectrons in surface-plasmon-assisted multiphoton photoelectric emission. *Phys. Rev. Lett.* **86**, 5180−5183 (2001).
31. Kupersztych, J. & Raynaud, M. Anomalous multiphoton photoelectric effect in ultrashort time scales. *Phys. Rev. Lett.* **95**, 147401 (2005).
32. Johnson, P. B. & Christy, R. W. Optical constants of noble metals. *Phys. Rev. B* **6**, 4370−4379 (1972).
33. Stockman, M. I., Bergman, D. J. & Kobayashi, T. Coherent control of nanoscale localization of ultrafast optical excitation in nanosystems. *Phys. Rev. B* **69**, 054202−10 (2004).
34. Nehl, C. L. *et al.* Scattering spectra of single gold nanoshells. *Nano Lett.* **4**, 2355−2359 (2004).
35. Goulielmakis, E. *et al.* Attosecond control and measurement: Lightwave electronics. *Science* (in the press).
36. Schnurer, M. *et al.* Guiding and high-harmonic generation of sub-10-fs pulses in hollow-core fibers at 10(15) w/cm$^2$. *Appl. Phys. B* **67**, 263−266 (1998).
37. Henke, B. L., Lee, P., Tanaka, T. J., Shimabukuro, R. L. & Fujikawa, B. K. Low-energy X-ray interaction coefficients: Photoabsorption, scattering, and reflection. *Atomic Data and Nuclear Data Tables* **27**, 1−131 (1982).
38. Manson, S. T. in *Photoemission in Solids* Vol. 1, (eds Cardona, M. & Ley, L.) 135−163 (Springer, Berlin, New York, 1978).
39. Tanuma, S., Powell, C. J. & Penn, D. R. Calculations of electron inelastic mean free paths. ii. Data for 27 elements over the 50−2000 eV range. *Surf. Interface Anal.* **17**, 911−926 (1991).

## Competing financial interests

The authors declare no competing financial interests.